Contents lists available at ScienceDirect

Construction and Building Materials

journal homepage: http://ees.elsevier.com

An experimental investigation of the mechanical strength of cold-drawn AISI 1018 steel under high-temperature steady- and transient-state conditions

Mohammad Badaruddin [a,*], Agus Sugiri [a], Chaur Jeng Wang [b]

[a] Department of Mechanical Engineering, Faculty of Engineering, Universitas Lampung, Jalan Prof. S. Brojonegoro No. 1, Bandar Lampung 35145, Indonesia
[b] Department of Mechanical Engineering, National Taiwan University of Science and Technology (NTUST), 43 Keelung Rd, Sec. 4, Taipei 106, Taiwan, ROC

ARTICLE INFO

Article history:
Received 9 April 2019
Received in revised form 13 September 2019
Accepted 6 October 2019
Available online xxx

Keywords
Cold-drawn mild steel
Steady-state
Transient-state
Mechanical strength
Fire resistance

ABSTRACT

Generally, in the event of a fire, steel structures exhibit different characteristics in terms of mechanical property degradation, which is significantly affected by the manufacturing of the steel. Therefore, the mechanical properties of cold-drawn AISI 1018 steel (CDS 1018) at elevated temperatures under steady- and transient-state conditions were investigated. The thermal expansion of CDS 1018 is relatively less than the thermal expansion predicted using Eurocode and ASCE standards at temperatures ranging from 25 to 650 °C. Dynamic strain ageing (DSA) improves the mechanical strength of CDS 1018 at steady-state temperatures ranging from 400 to 500 °C. Under transient-state conditions, the mechanical strength of CDS 1018 is better than those of high-strength steel (HSS) and ultrahigh-strength steel (UHSS) grades in the temperature range of 500–600 °C. Application of the cold-drawing process to AISI 1018 steel provides thermal creep resistance at temperatures up to 600 °C. The current design standards from the Eurocode, ASCE and AISC cannot be adapted for the fire-resistant design of structural mild steel delivered by cold-drawing conditions. Therefore, the present experimental data series obtained from steady- and transient-state methods are applicable to predict the mechanical degradation of CDS 1018 for engineering applications in fire-safety design.

1. Introduction

In this century, structural steel is becoming an increasingly essential construction material and the main choice for components of modern buildings across all construction building sectors, such as apartments, centres of business, and private companies. In the widespread use of structural steel as a building material, the fire-safety design of structural steel is the main criterion required to ensure that fire events within a building do not cause the structures of that building to collapse in short periods of time, thereby allowing all the occupants to be evacuated. Regarding structural steel applications, many researchers have evaluated the performance of structural steel on the basis of steel strength: regular steel grades with a yield strength of 250–350 MPa, high-strength steel (HSS) grades with a yield strength of 460–700 MPa, and ultrahigh-strength steel (UHSS) grades with a yield strength exceeding 700 MPa. Kirby and Preston [1] have provided elevated temperature data for two hot-rolled mild steels with yield strengths of 250 MPa (steel 43A grade) and 350 MPa (steel 50B grade) under steady- and transient-state conditions for applications in structural fire engineering design. Chen et al. [2] have reported that the reductions in yield strength and elastic modulus of hot-rolled XLERPLATE Grade 350 and of quenched HSS BISPLATE 80 grade at temperatures ranging from 22 to 540 °C are quite similar. Knobloch et al. [3] have found that the mechanical behaviour of both rectangular hollow sections and hot-rolled wide-flange sections of grade S355 are markedly affected by any given strain rate from 0.02 to 0.5%/min in steady-state elevated temperature tests. Furthermore, Neuenschwander et al. [4] confirmed that the mechanical property degradation of hot-rolled round bars of S355J2 grade under normalizing conditions at steady-state temperatures from 400 to 900 °C can be predicted with adequate accuracy by the EC3 [5] and ASCE [6] design standards. By contrast, for light gauges of cold-formed mild steel structures of grades G550 and G250, Ranakawa et al. [7] have proposed a new model for accurately predicting the mechanical properties for safe design under fire conditions via stress-strain curve relationships.

Furthermore, recently, the use of HSS grades for building construction has increased more than that of regular steel due to the high strength-to-weight ratio of building components. In addition, in high-rise construction buildings, the need for steel is lessened by using single support or beam structures, which lead to decreased material costs and improved sustainability of HSS production. The HSS grades are classified on the basis of nominal yield strengths between 460 MPa and

* Corresponding author.
E-mail address: mbruddin@eng.unila.ac.id (M. Badaruddin)

https://doi.org/10.1016/j.conbuildmat.2019.117193
0950-0618/

700 MPa [5]. For example, a hot-rolled steel plate with a thickness of 5 mm under normalizing conditions has a yield strength of 460 MPa, and its strengthening was achieved by adding micro-alloying elements such as Nb, Ti and Ni, the steel grade of which is S460NL [8]. In the study by Qiang et al. [8], they used HSS S460NL and reported that the degradation of the mechanical properties of S460NL at elevated temperatures under steady- and transient-state conditions is not addressed by the current design standards of EC3 [5] and the AISC [9] and is considerably dependent on the steel grade. Steel with a yield strength of approximately 700 MPa and appropriate ductility is generally obtained by adding alloying elements at a low concentration of 0.1 wt% or less and subjecting the steel to quenching and tempering (Q&T) heat treatments [10-12] and combinations of Q&T and thermo-mechanical control processes (TMCPs) [13,14]. The delivery process for UHSS S960 grade, the yield strength of which exceeds 700 MPa, under Q&T conditions is similar [15,16]. It is generally found that the degradation of HSS grades [10-15] and UHSS grades [15,16] at elevated temperatures can be related to the formation of martensite in the initial microstructure, which is similar to the finding of Heidarpour et al. [17] that the low thermal stability of the martensite phase results in a rapid reduction in the strength of UHSS due to the formation of large precipitates comprising soluble carbides containing chromium and molybdenum [15]. Therefore, the greater reduction in mechanical strength of HSS and UHSS grades than mild steel at elevated temperatures can be attributed to the difference in the initial steel microstructures.

In the present study, we focused on investigating the mechanical properties of cold-drawn AISI 1018 steel under steady- and transient-state conditions at elevated temperatures. Numerous studies have focused on the mechanical properties of regular steel grades [1-4,7], HSS grades [8,10-15], UHSS grades [15-17], cold-formed hollow steel tubes [18] and cold-drawn wire steel and cable [19,20], which differ in their chemical compositions and manufacturing processes and the conditions of the testing methods under steady- and transient-state conditions. The transient-state test method has been found to be more realistic than the steady-state test method in simulations investigating mechanical behaviours under fire conditions. However, the stress-stain curves obtained from converting the strain-temperature curve are from different specimens [10], and coupling strain, generated from a combination of stress, temperature, and thermal creep [21], leads to nonlinear-elastic behaviour of steel. Consequently, the calculated values of the elastic modulus and yield strength are sometimes underestimated. By contrast, in steady-state high-temperature tensile tests, the elastic modulus, yield strength and ultimate strength values are obtained directly from stress-strain curves [7,8]. Therefore, the possible errors during the determination of the mechanical properties of steel can be reduced. Furthermore, the present test results were compared with existing data from previous studies on HSS grades [8,10-15], UHSS grades [15,16], cold-formed hollow steel tubes [18] and cold-drawn wire steel and cable [19,20] under high-temperature steady- and transient-state conditions available in the literature. The current design standards available from the Eurocode [5,22], ASCE [6] and AISC [9] are also compared to the present data test results.

Table 1
Chemical compositions of CDS 1018.

C	Si	Mn	P	S	Cr	Mo
0.152	0.344	0.872	0.0228	0.0062	0.0307	0.0037
Ni	Al	Co	Cu	Ti	Sn	Nb
0.0262	0.0440	0.0083	0.0171	0.0253	0.0047	<0.004

2. Experimental procedure

2.1. Materials and test equipment

In the present study, all the specimens were obtained from commercial AISI 1018 steel with a diameter of 12 mm under cold-drawing conditions. The chemical compositions of the cold-drawn AISI 1018 (CDS 1018) (wt%) are displayed in Table 1. The tensile specimens were machined according to ASTM standard E8M [23] using a CNC lathe with an EmcoTronic TM02 controller. The specimen dimensions and photographs are shown in Figs. 1 and 2, respectively. An MTS Landmark material testing machine with a capacity of 100 kN and a mobile mini-furnace with a temperature controller with an accuracy of $\pm 1\,^{\circ}C$ were used in the experimental procedures (Fig. 3). The furnace with a maximum working temperature of 1200 °C has two hot zones with two silicon carbide heating elements in each zone. Two K-type thermocouples attached to the specimen were used to control the temperature during testing. A high-temperature extensometer with two alumina extension rods and a gauge length of 12 mm was used to measure axial strain at high temperatures. The ceramic extension rods were extended into the hot zone, and the tips of the ceramic rods contacted the specimen, as shown in Fig. 3.

2.2. Tension and thermal strain tests at elevated temperatures

In the present research, two series of tests were performed for CDS 1018 at high temperatures: tensile tests under steady-state conditions and transient total deformation tests. The axial strains at room temperature (RT ≈ 25 °C) and at elevated temperatures (100–750 °C) were

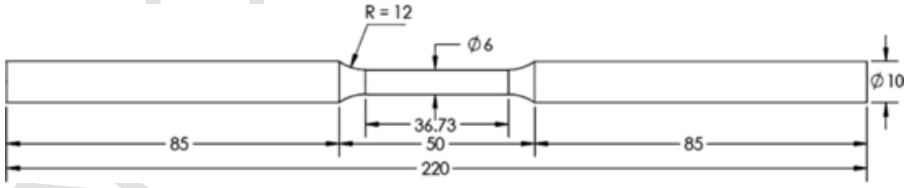

Fig. 1. Dimensions of the tensile specimens (all in mm).

Fig. 2. Photographs of the tensile specimens.

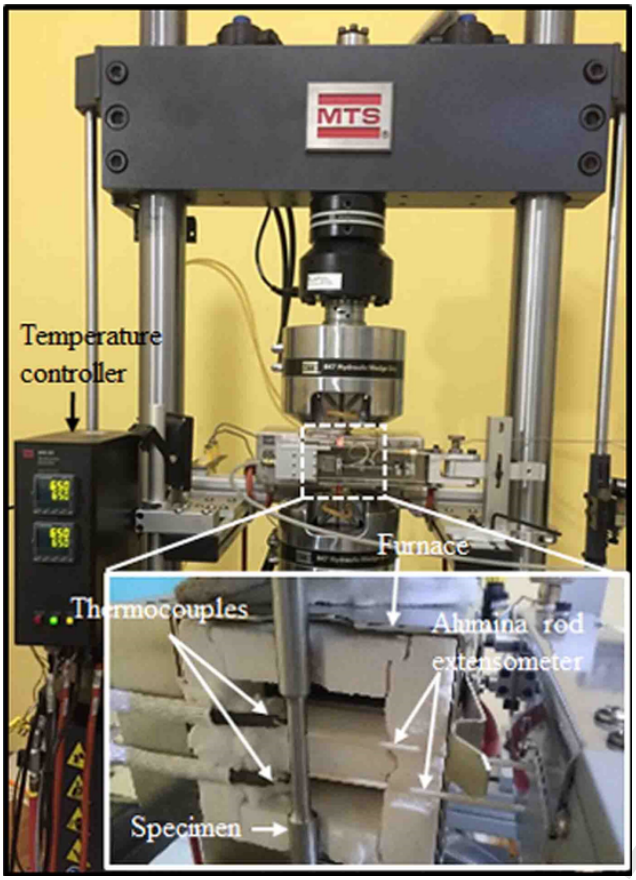

Fig. 3. Detailed view of the experimental setup: positions of the thermocouples and mounting extensometer on the specimen.

measured using an extensometer with a gauge length of 10 mm and a high-temperature extensometer with a gauge length of 12 mm, respectively. The specimen temperatures were recorded using two thermocouples (XCIB K-type series from Omega) attached to the specimen in the gauge length region, as recommended by ASTM E21 [24] and as shown in Fig. 3. The specimen temperature is an average value obtained by temperature measurements from both thermocouples. To avoid breaking the alumina rod extensometer, the extensometer removal point was set to 0.02 mm/mm.

The steady-state tensile tests had 10 temperature levels: 100 °C, 200 °C, 300 °C, 400 °C, 500 °C, 550 °C, 600 °C, 650 °C, 700 °C and 750 °C. The template for tensile testing at steady-state high temperatures was especially created to run the tensile testing programme according to ASTM standards E8 [23] and E21 [24]. Each experiment at the test temperature was repeated three or seven times with a total of 50 samples. Details on the number of specimens used in the present research for the different types of tests are displayed in Table 2. In the steady-state tensile tests, the specimen was heated by controlling the heating rate at 20 °C/min until the test temperature was reached and then maintained for a soak time of 35 min. Before the start of the tests, the axial strain was offset to zero, and the specimen was axially tensioned under displacement control at a constant speed of 0.18 mm/min and a certain test temperature until the specimen failed. The elastic modulus, 0.2% yield strength and ultimate strength were automatically determined using the tensile test template of the MTS software program. The stress-strain data series for the segment length of the 20% elastic curve were automatically recorded to determine the elastic modulus of the steel [25] using the template test program. The strain rate obtained from the axial strain vs. run time plot was approximately

Table 2
The detailed number of specimens used in different types of tests.

Type of tests	Number of specimens	Control system		
		Displacement rate (mm/min)	Force rate (kN/s)	Heating rate (°C/min)
Tension at RT	7	0.18	–	–
Thermal strain	3	–	–	10
Steady-state	43	0.18	–	20
Transient-state	37	–	0.08	10

0.003/min, which satisfied the requirements of ASTM standard E21 [24]. In the steady-state tests, all the incremental strains up to 0.02 mm/mm were recorded to plot the stress-strain relationship curve.

In the transient total deformation tests, the specimen was initially loaded to a desired level of stress (stress levels of 50, 100, 150, 200, 250, 300, 350, 400, 500 and 520 MPa for CDS 1018 were chosen) under a constant load rate of 0.08 kN/s. When the steel was at the stress level, the furnace was turned on. In the transient temperature tests, the specimen temperature in the furnace was increased at a constant heating rate of 10 °C/min until the specimen failed. A similar heating rate of 10 °C/min for the HSS S690QL grade [10] and UHSS S960QL grade [16] was used in the experiments, in which a heating rate of 10 °C/min is equivalent to a 1-hour standard fire resistance test [1]. Three specimens were tested in each transient-state experiment, except for the 250 MPa and 300 MPa stress levels, for which four specimens were used. The total number of specimens for the transient-state experiments was 37, as displayed in Table 2.

In the thermal strain tests, the specimen was gripped in a zero-load condition, and the extensometer was attached to the gauge region of the specimen. During the thermal strain tests, an axial force was maintained in a zero-load condition, and the actuator was allowed to undergo axial displacement. The increasing temperature in the furnace was controlled by two thermocouples at a constant heating rate of 10 °C/min until the specimen temperature was 800 °C. Thermal strain tests, tensile tests in steady-state temperatures and total deformation tests at transient temperatures were run using a personal computer with different test templates in MTS Multipurpose Elite (MPE) software. Recording during data acquisition (DAQ), which consisted of measuring the specimen temperature, axial strain, axial force, displacement, and run time at a sampling frequency of 10 Hz, was performed by employing MTS MPE software.

3. Results and discussion

3.1. Analysis of thermal strain

The average values of the thermal strain from the three specimens of CDS 1018 tested per temperature are presented in Table 3. Fig. 4 displays the temperature-thermal strain relationship for CDS 1018 and comparisons with thermal strain values from the literature [2,20] and data model predictions from the Eurocode design standard for cold-drawn wire steel (EC2) [22] and for mild steel (EC3) [5] and from the ASCE [6]. Data model predictions from the ASCE and Eurocode are not applicable for accurately predicting the thermal expansion of AISI 1018 steel under cold-drawing conditions or of HSS BISPLATE 80 grade under quenching conditions [2]. Steel cable data [20] exhibit slight deviations from the data model predictions from EC2 in a temperature range of 100–450 °C in Fig. 4. A larger discrepancy was observed at

Table 3
Thermal strain of CDS 1018 at different temperatures.

Temperature (°C)	25	100	200	300	400	500	550	600	650	700	750	800
Thermal strain ($\times 10^{-3}$) (mm/mm)	0.017	0.310	0.620	1.046	1.666	2.499	3.026	3.624	4.316	7.319	10.383	12.520

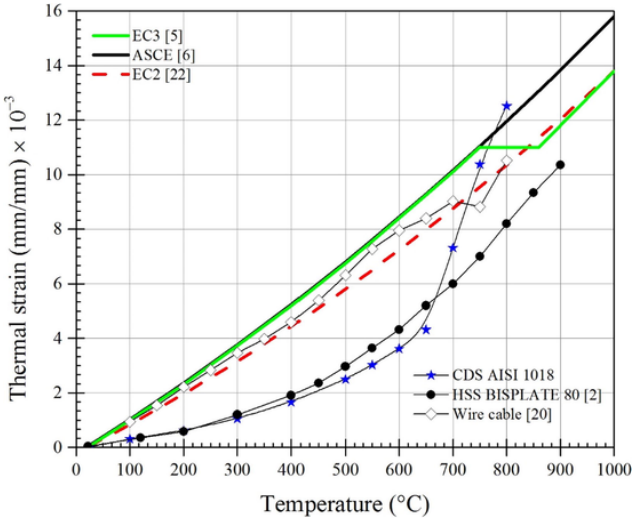

Fig. 4. Comparison of the thermal strain of CDS 1018 with data model predictions of the Eurocode and ASCE, CDS wire cable and high-strength BISPLATE 80 steel.

550 °C, and then the thermal strain was relatively constant in the 700–750 °C temperature range, which can generally be related to the onset of the phase transformation of ferrite to austenite by absorption of a large amount of heat [20]. The comparisons of the thermal strain values from data model predictions [5,6,22] and the literature [20] in Fig. 4 to the present test results show that the thermal strain in the temperature range of 25–650 °C is higher. Compared with that of HSS BISPLATE 80 grade, the thermal strain of CDS 1018 shows relatively identical values [2] in the temperature range of 25–300 °C and exhibits lower values in the temperature range of 400–650 °C. Neunschwander et al. [4] reported that regardless of the manufacturing of the steel grades, the thermal strain of hot-rolled steel of grade S355J2 under normalizing conditions is lower than the data model prediction of the thermal strain from the ASCE and EC3 at temperatures up to 900 °C. In addition, the thermal expansion trends of both HSS S690QL grade and UHSS S960QL grade under Q&T conditions are nearly the same at temperatures up to 600 °C [15]. It is clear that the chemical composition and manufacturing of steel lead to different thermal expansion behaviours.

As indicated by the above review of the literature, AISI 1018 steel under cold-drawing conditions shows different behaviour; therefore, the present data in Table 3 can be used to develop a model prediction of the temperature-thermal strain relationship in the temperature range of 25–800 °C. The predictive equations of this model are presented as Eq. (1).

$$\epsilon_{th} = 1.071 \times 10^{-13} T^4 - 1.011 \times 10^{-10} T^3 + 3.220 \times 10^{-8} T^2 + 3.318 \times 10$$

The thermal expansion coefficient (α_T) of CDS 1018, which describes the axial deformation change in size and per degree change in temperature [20], can be determined by differentiating Eq. (1) as follows:

$$\alpha_T = \frac{d\epsilon_{th}}{dT} = 4.284 \times 10^{-13} T^3 - 3.033 \times 10^{-10} T^2 + 6.440 \times 10^{-8} T + 3.31$$

The thermal expansion coefficient of CDS 1018 determined by using Eq. (2), shows nonlinear behaviour in the temperature range of 25–800 °C.

3.2. Analysis of the test results

Fig. 5 shows the stress-strain curves of CDS 1018 at different steady-state temperatures. Typical axial force-displacement curves are displayed in Fig. 6. The static drop caused by pausing the motion of

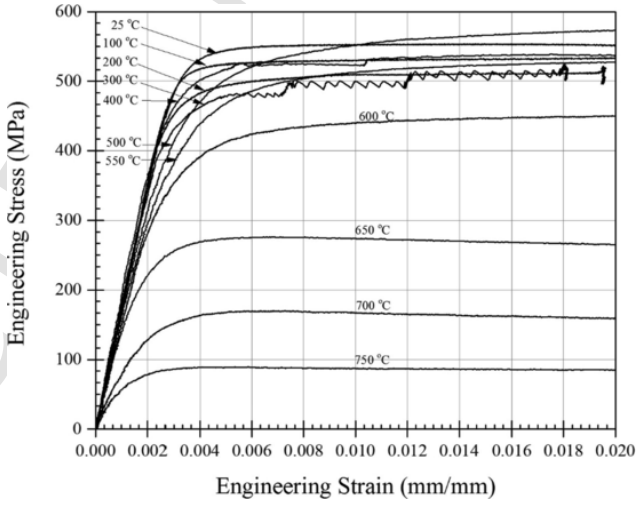

Fig. 5. Stress-strain curves of CDS 1018 at elevated temperatures.

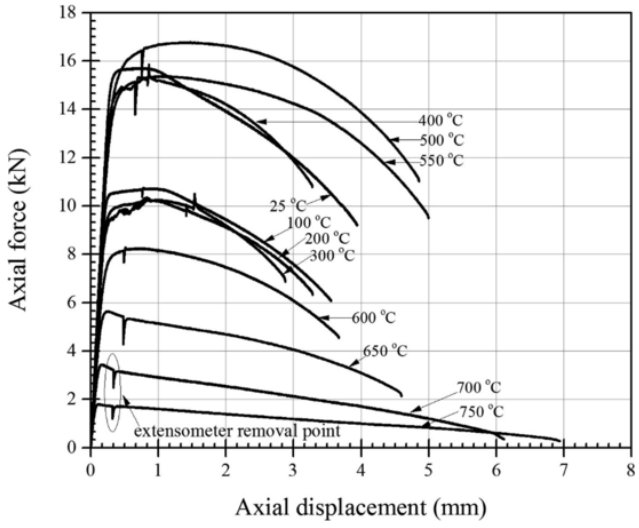

Fig. 6. Typical axial force-displacement curves for CDS 1018 at elevated temperatures under steady-state conditions.

the actuator for a few seconds to release the extensometer from the specimen is observed in Fig. 6. However, a static force drop effect of a few seconds can be neglected [2]. In room temperature tests, CDS 1018 exhibits linear behaviour in the plastic portion of the force-displacement relationship in Fig. 6. CDS 1018 does not exhibit a well-defined yield point, which is similar behaviour to that of high-strength prestressing steel [26] and high-strength cold-formed hollow steel tubes [27] at room temperature. Furthermore, in the temperature range of 200–300 °C, the steel underwent relatively small strain hardening (Fig. 6). Significant strain hardening was observed in CDS 1018 at an onset temperature of 400 °C up to a final temperature of 500 °C, as shown in Fig. 6. Furthermore, under subsequent tensile deformation, CDS 1018 exposed to a higher temperature of 550 °C experienced a rapid decay of mechanical strength due to recovery and recrystallization processes.

Fig. 7 displays typical temperature-strain curves of CDS 1018 after transient total deformation tests. The failure temperature is defined as the fire temperature at which the steel specimen fails at a constant stress level. The average failure temperatures of CDS 1018 at various stress levels up to 520 MPa (~$0.95f_y$) obtained from each transient deformation test are presented in Table 4. In the stress level range of 50–520 MPa, CDS 1018 can withstand a fire temperature >600 °C. However, when CDS 1018 specimens were loaded up to an approximate stress level of 525 MPa, the steel failed under low-temperature deformation below 100 °C. This phenomenon was attributed to the relatively low load-deformation capacity of CDS 1018. The application of cold drawing to mild steel results in elongation of the grains of ferrite and pearlite in the longitudinal axis of the steel [26]. In addition, the highly deformed lamellar cementite (Fe_3C) of pearlite in the ferrite matrix decreased the interphase spacing between lamellar structures and ferrite [28]. Low interphase spacing provides a large boundary area, which effectively enables dislocation motion to be blocked, leading to an increase in high dislocation density. Therefore, dislocation-strain hardening generates a large compressive residual stress in the axial direction [29,30]. Thus, the mechanical strength of AISI 1018 increased significantly. In contrast, this steel has a low capacity for plastic deformation during tensile deformation at room temperature. Therefore, we can conclude that when AISI 1018 under cold-drawing conditions is loaded until the nominal yield strength reached, CDS 1018 becomes susceptible to thermal deformation with increasing temperature.

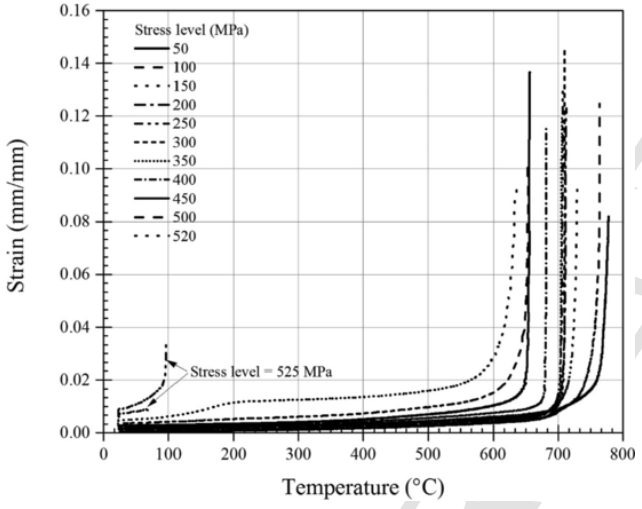

Fig. 7. A typical temperature-strain relationship of CDS 1018 steel at different stress levels.

Table 4
Failure temperatures of CDS 1018 after transient total deformation tests.

Stress level (MPa)	Failure temperature (°C)
50	782
100	769
150	732
200	713
250	708
300	691
350	688.5
400	682.5
450	657
500	654
520	637
525	<100

Under transient-state conditions, the mechanical properties of CDS 1018 were determined using a similar procedure to that employed by Qiang et al. [10] in their previous research. Typical stress-strain curves of CDS 1018 experimentally established from the present test series are displayed in Fig. 8, in which the stress-strain curves in the elastic portion show nonlinear behaviour. Therefore, the elastic modulus of CDS 1018 is conventionally determined using the tangent modulus [25], and the yield strength is determined using a 0.2% strain offset method [23].

In the present study, the elastic modulus, yield strength, and ultimate strength obtained in the room temperature tests are represented by E, f_y, and f_u, respectively, and those obtained in the elevated temperature tests are represented by E_T, f_{yT}, and f_{uT}, respectively. The ratios of the elastic modulus, yield strength and ultimate strength obtained at the test temperatures to those obtained at room temperature are defined as the reduction factor. The temperature dependence of the mechanical properties of CDS 1018 under steady-state and transient-state conditions was evaluated on the basis of the concept of reduction factor-temperature relationships. The mechanical properties of CDS 1018 and the reduction factors at elevated temperatures under steady- and transient-state conditions obtained from an average value of each experiment's test data are given in Tables 5 and 6.

Fig. 9a displays a comparison of the reduction factor of the elastic modulus under steady- and transient-state conditions, where a significant difference in the reduction factor is observed only at temperatures >300 °C. Furthermore, in the temperature range of 400–750 °C, the reduction factors of the elastic modulus calculated under steady-state conditions are higher (~6.6–91.0%) than those calculated under tran-

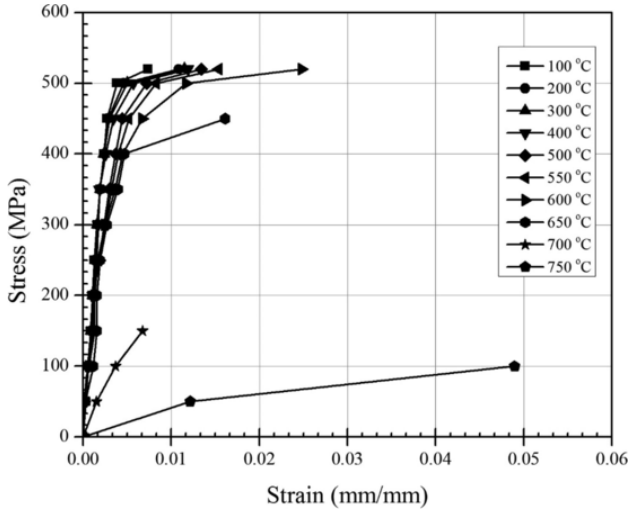

Fig. 8. A typical stress-strain curve of CDS 1018 under transient-state conditions.

Table 5
The values of the mechanical properties of CDS 1018 corresponding to their reduction factors under steady-state conditions.

Temperature (°C)	E (GPa)	f_y (MPa)	f_u (MPa)	Reduction factor		
				E_T/E	f_{yT}/f_Y	f_{uT}/f_u
25	197.067	545.331	550.644	1.000	1.000	1.000
100	186.709	508.682	524.336	0.947	0.933	0.952
200	176.830	505.226	525.942	0.897	0.926	0.955
300	177.256	489.701	529.656	0.899	0.898	0.962
400	174.439	499.616	554.124	0.885	0.916	1.006
500	171.253	502.204	580.064	0.869	0.921	1.053
550	168.543	463.216	531.296	0.855	0.849	0.965
600	158.318	393.645	445.641	0.803	0.722	0.809
650	140.526	279.606	296.813	0.713	0.513	0.539
700	97.919	160.989	171.875	0.497	0.295	0.312
750	80.666	73.919	84.993	0.409	0.136	0.154

Table 6
The values of the mechanical properties of CDS 1018 corresponding to their reduction factors under transient-state conditions.

Temperature (°C)	E (GPa)	f_y (MPa)	f_u (MPa)	Reduction factor		
				E_T/E	f_{yT}/f_Y	f_{uT}/f_u
25	197.067	545.331	550.644	1.000	1.000	1.000
100	189.363	508.301	520.000	0.961	0.932	0.944
200	176.244	502.450	520.000	0.894	0.921	0.944
300	175.733	501.547	520.000	0.892	0.920	0.944
400	163.054	500.848	520.000	0.827	0.918	0.944
500	149.731	497.593	520.000	0.760	0.912	0.944
550	132.133	496.631	520.000	0.670	0.911	0.944
600	114.131	495.272	520.000	0.579	0.908	0.944
650	75.438	408.443	450.000	0.383	0.749	0.817
700	31.309	143.751	150.000	0.159	0.264	0.272
750	7.217	46.461	100.000	0.037	0.085	0.182

sient-state conditions. Fig. 8 provides evidence that temperature degrades CDS 1018 in a complex manner due to the interactive effects of temperature, load, thermal creep and microstructural changes [31].

At temperatures ≤500 °C, the reduction factors of the yield strength calculated by the two methods are almost identical, as shown in Fig. 9b. However, at T = 550 °C, 600 °C and 650 °C, the reduction factors of the yield strength calculated for the steady-state test condition are 6.8%, 20.5% and 31.5%, respectively, lower than those calculated under the transient-state condition. In the 700–750 °C temperature range, the reduction factors of the yield strength obtained from the two methods are quite similar. Furthermore, the reduction factors of the ultimate strength obtained from the two methods at temperatures ≤300 °C are almost identical, as shown in Fig. 9c. As the temperature increases from T = 400 °C up to T = 500 °C, the ultimate strength under steady-state conditions increases significantly. The gradual increase in the strength from 400 to 500 °C was attributed to dynamic strain ageing (DSA), which is indicated by the plateau in the variation in ultimate strength in the temperature range of 200–500 °C in Fig. 9c. Again, at T = 550 °C, the reduction factor of the ultimate strength had almost the same value. However, at T = 600 °C and 650 °C: the ultimate strength values under transient-state conditions are 15.2% and 12.7%, respectively, higher than the ultimate strength values under steady-state conditions, respectively. Fig. 9b and c demonstrate that CDS 1018 experienced a higher reduction in the mechanical strength under steady-state conditions than under transient-state conditions in the temperature range of 600–650 °C. This phenomenon is mainly because both the relatively high thermal deformation capacity of CDS 1018 under ~0.95f_y

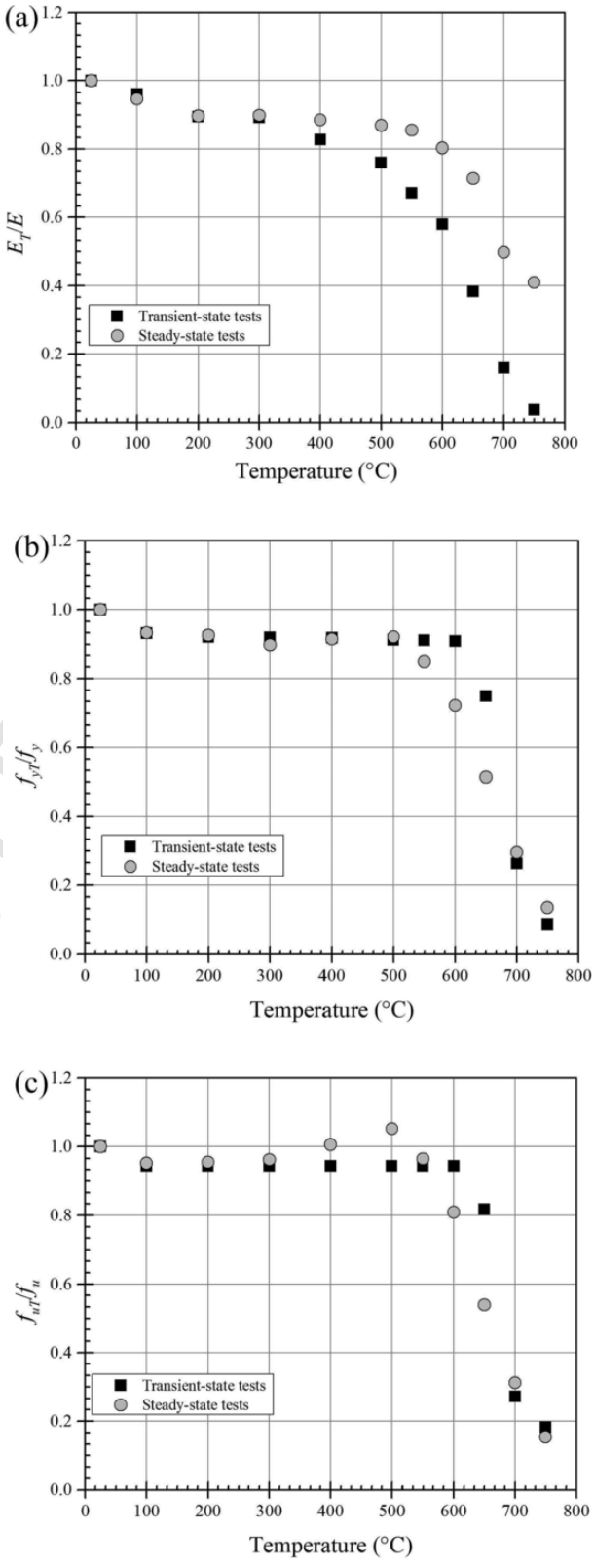

Fig. 9. Comparisons of the reduction factor-temperature relationship: (a) elastic modulus, (b) yield strength, and (c) ultimate strength under steady- and transient-state conditions.

loading and its low thermal expansion enable it to withstand high transient temperature deformation. Therefore, CDS 1018 experiences fire failure at temperatures higher than 600 °C, which is evidenced by Fig. 7 and has a considerable influence on the mechanical strength of the steel.

Furthermore, the reduction factors with the temperatures experimentally obtained using steady- and transient-state methods from the present work and previous works available in the literature [8,10-16,18] are compared together with the current design standards from the Eurocode [5,22], ASCE [6] and AISC [9]. Comparisons are presented in each figure displaying the reduction factor-temperature relationships of the elastic modulus, yield strength and ultimate strength for HSS and UHSS grades. Each figure presents two parts: (a) the left part demonstrates the comparison of HSS grades with a nominal yield strength (f_y) between 460 and 700 MPa ($f_y \langle 700$), and (b) the right part demonstrates the comparison of UHSS grades with a nominal yield strength exceeding 700 MPa ($f_y > 700$). Data for each steel grade from the literature in the respective figures of the reduction factor-temperature relationship are included using the envelope indicated by light grey shading to emphasize the relation of the present test data to data from the literature. Additionally, data sets of reduction factors of the mechanical properties of cold-drawn wire strand [19] and cable [20] are also included in separate envelopes in each figure of part b. Data sets from the experimental works available in the literature were taken into account in the data set for this comparative study and are listed in Table 7.

3.3. Comparative analysis of test results in steady-state condition

3.3.1. Elastic modulus

The present data and data in the envelope in Fig. 10a reveal that temperature induces a reduction in the elastic modulus of HSS grades and CDS 1018. The reduction in the elastic modulus of CDS 1018 is slightly higher than the reduction in the elastic modulus of HSS grades [11,13–15,18] in the temperature range of 100–400 °C, as shown in Fig. 10a. However, compared to the reduction in the elastic modulus of HSS grades, the reduction in the elastic modulus of CDS 1018 exhibits a relatively slow rate in the temperature range from 100 to 550 °C. Although the CDS 1018 data in Fig. 10a show considerable discrepancies, the data still lie in the envelope. Increasing the temperature from 200 to 800 °C degraded the RQT 701 steel [12] at a much higher rate. Data from [11,14,15,18] in the envelope demonstrate intense degradation at an onset temperature of 400 °C, except for the Q690 CFD steel from [13], the reduction rate of which is slow up to a temperature of 500 °C. Furthermore, the data in the envelope in Fig. 10b reveal that the temperature severely degraded the S960QL grade steel [15,16], ultrahigh-strength square hollow section of tubes (SHS900) [18] and wire strand [19] and steel cable [20] at an initial temperature of 300 °C.

HSS grades and CDS 1018 in the present do not obey conservative predictions regarding the reduction in the elastic modulus-temperature relationship from the curve models of the EC3 and ASCE in Fig. 10a. However, the data for RQT 701 steel [12] are slightly overlapping with those for the ASCE from 100 to 500 °C and continue to be conservative again relative to the EC3 in the range from 600 to 800 °C. The weighted centreline of the envelope established from the experimental results of the test series from the literature in Fig. 10a does not show a better match with the curve model predictions of the EC3 and ASCE. However, the data from [11,14,18] appear to be nearly underestimated relative to the weighted centreline of the envelope. The wire strand and steel cable data in the envelope in Fig. 10b are not conservative relative to the curve model predictions of the EC2. In contrast, the UHSS S960QL grade [16] in the range of 100–700 °C and SHS900 [18] in the range of 450 to 800 °C are conservative relative to the EC3 and ASCE, respectively. The large disparities of elastic behaviour at high temperatures in Fig. 10a and b are attributed to the steel chemical

Table 7
Summary of previous work available in the literature for HSS and UHSS grades.

Reference	Steel grade	Manufacturing process	Test method	Control system			
				Displacement or force	Strain rate (%/min)	Heating rate (°C/min)	Temperature range (°C)
Qiang et al. 2013 [8]	S460NL	HR + N	S&T	n.a [b,d]	0.5 [a]	50 [a], 10 [b]	20–700
Qiang et al. 2012 [10]	S690QL	Q&T	S&T	n.a [b,d]	0.5	10 [b]	20–700
Chiew et al. 2014 [11]	RQT S690	Q&T	S	0.2 [c]	–	20	25–800
Xiong and Liew 2016 [12]	RQT 701	Q&T	S&T	0.15 [a], 1.5 [b,d] kN/min	–	10 [a,b]	30–800
Jiang et al. 2019 [13]	Q690CFD	TMCP + Q&T	S	10	1–10	n.a	30–900
Choi et al. 2014 [14]	HSA800	TMCP + Q&T	S	–	0.4 [e], 1.5 [f], 0.8 [g]	10	25–900
Neuenschwander et al. 2017 [15]	S690QL, S960QL	HR + Q&T Q&T	S	–	0.2	15	20–900
Qiang et al. 2016 [16]	S960QL	Q&T	S&T	n.a [b,d]	0.5	50 [a], 10 [b]	20–700
Li and Young 2017 [18]	Tubes hollow steel	Cold-forming	S&T	0.3 [a]	–	50 [a], 10 [b]	~21–1000
Shakya and Kodur 2016 [19]	Wire strand	Cold-drawing	S	60 [d] MPa/min	–	10	20–800
Du et al. 2018 [20]	Wire cable	Cold-drawing	S	–	0.3	10	20–800

HR is hot rolling, Q is quenching, T is tempering, N is normalizing, TMCP is thermal-mechanical control process, S is steady-state condition and T is transient-state condition.
[a] Steady-state condition.
[b] Transient-state condition and n.a is not available.
[c] Displacement rate (mm/min) and
[d] force rate.
[e] Until yield point in range 20–900 °C,
[f] Beyond yield point in range 100–400 °C and
[g] Beyond yield point in range 500–900 °C.

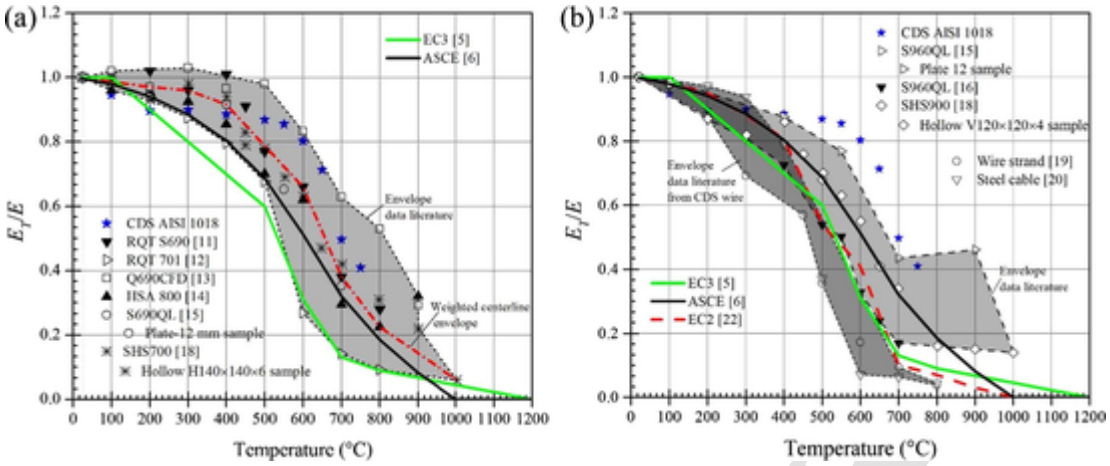

Fig. 10. Comparison of the reduction factor–temperature relationship of the elastic modulus under steady-state conditions for different steel grades: (a) $f_y < 700$ and (b) $f_y > 700$.

compositions, which lead to differences in the initial microstructure, as the microstructures have important implications for high-temperature steel properties and creep resistance [32,33]. Therefore, some of the data in envelopes of Fig. 10a and b show a nonconservative trend relative to data model predictions of the Eurocode (EC2 and EC3) and ASCE. The manual of the Eurocode design standard implicitly inserted thermal creep effects from transient total deformation experiments for accurately predicting the degradation of structural steel in a fire.

3.3.2. Yield strength

The reduction factor values of the yield strength of CDS 1018 were compared with those of HSS grades [11–15,18], UHSS grades [15,16,18] and cold-drawn wire strand and cable [19,20] in Fig. 11a and b. The data in the envelopes in Fig. 11a and b show considerable discrepancies with the present data from the different temperature tests. The yield strength reduction data in Fig. 11a reveal that HSS grades under Q&T conditions [12–14] and square hollow steel tubes under cold-forming conditions (SHS700) [18] experienced lower reductions than that of AISI 1018 steel under cold-drawing conditions (CDS 1018) in the temperature range of 100–300 °C. However, the yield strength of CDS 1018 initially slowly decreases with increasing temperature up to 300 °C and then gradually increases at temperatures up to 500 °C; beyond this temperature, a rapid degradation in yield strength is observed up to a temperature of 750 °C. The rapid degradation of HSS grades [12-15] and SHS700 [18] occurs at the onset temperature of 400 °C.

Furthermore, some of the data [16,18] in Fig. 11b show rapid degradation at the onset temperature of 300 °C. However, rapid degradation of wire strand [19] and cable steel [20] starts at 200 °C until the final degradation occurs at 800 °C. The data from Neunschwander et al. [15] and Qiang et al. [16] show a similar trend from 400 to 900 °C. The data in the envelopes in Fig. 11a and b evidently demonstrate that the degradation of steel at elevated temperatures can be related to the chemical compositions and manufacturing of the steel. The strengthening in S690 grade steel [12-15] and S960QL grade steel [15,16] can generally be related to the formation of both martensite tempering and finely dispersed particles of carbides containing Nb, Ni or Ti in the initial microstructure. The martensite structure and finely dispersed particles of Nb, Ni or Ti carbides are able to decelerate the degradation of the mechanical strength at a slow rate at temperatures below 400 °C, which is evident in Fig. 12a. However, the martensite in the S960 grade steel at temperatures higher than 300 °C tends to weaken the mechanical strength of the steel due to the solute diffusion of carbon atoms into the grain boundary to form carbides containing Mo and Cr [15], which cause Cr and Mo depletion in the ferrite matrix. Therefore, the chemical compositions and manufacturing of steel grades result in different microstructures, which considerably affect the behaviour of steel at elevated temperatures. These aspects are two important factors contributing to the performance of HSS and UHSS steel grades at elevated temperatures, which is sometimes found to be nonconservative or less conservative relative to the curve model predictions of the Eurocode and ASCE.

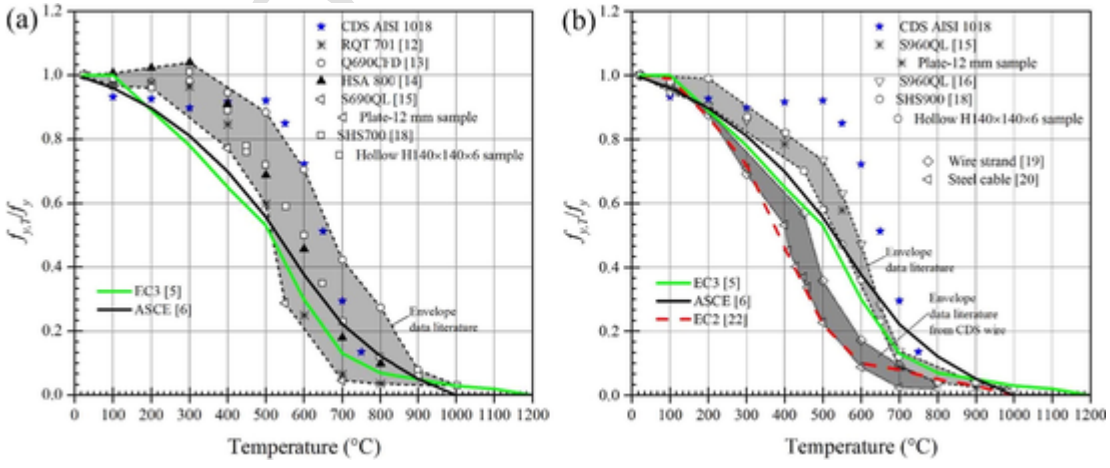

Fig. 11. Comparison of the reduction factor–temperature relationship of the yield strength under steady-state conditions for different steel grades: (a) $f_y < 700$ and (b) $f_y > 700$.

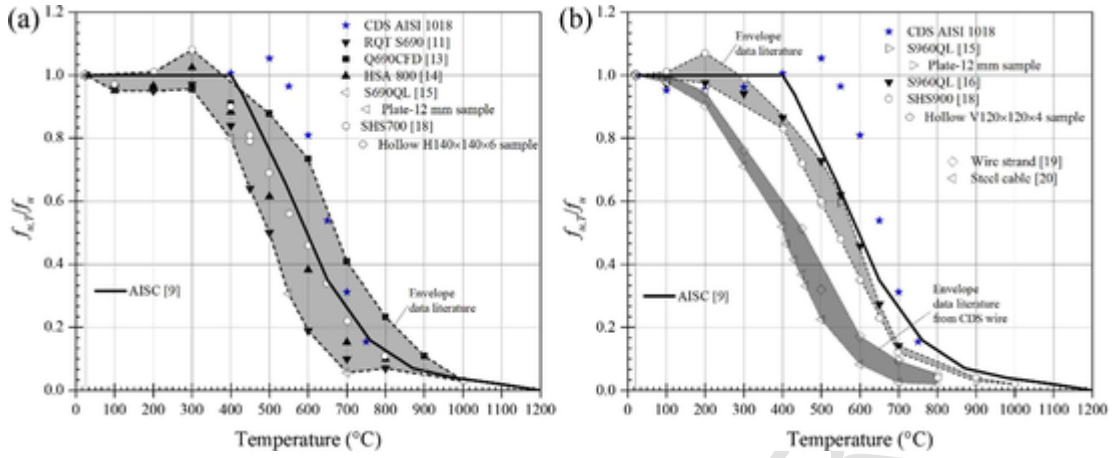

Fig. 12. Comparison of the reduction factor–temperature relationship of the ultimate strength under steady-state conditions for different steel grades: (a) $f_y < 700$ and (b) $f_y > 700$.

3.3.3. Ultimate strength

The reduction factors of the ultimate strength of CDS 1018 were compared with those of HSS grades and UHSS grades in Fig. 12a and b, respectively. The degradation of CDS 1018 occurs at nearly the same rates as the degradation of high-strength RQT S690 steel [11] and Q690CFD steel [13] in the temperature range of 100–300 °C. Some of the data [14,18] show a plateau or even a peak in the temperature range of 200–300 °C, which indicates that the blue brittleness phenomenon was induced in the steel. At the onset temperature of 400 °C, CDS 1018 begins to exhibit better performance than those of HSS grades until the ultimate strength reaches a peak exceeding a magnitude of 1.0 at 500 °C due to DSA. The peak of strain hardening in CDS 1018 occurring at 500 °C results in an advantageous effect on the increased ultimate strength and ductility, which can be closely related to interactions of dissolved carbon atoms from highly deformed pearlite and dislocations in the ferrite matrix [34]. However, Neuenschwander et al. [4] reported that the DSA induced in a round bar of a 150 mm solid section and a 60 mm solid section of hot-rolled mild steel of grade S355 under normalizing conditions at 400 °C were related to the high manganese content in both steels. This characteristic is generally similar to those of HSS grades [13-15,18]. At T > 300 °C, a higher 1.0 wt% Mn content in high-strength mild steel grades strongly leads to anisotropy of the tensile properties due to the formation of elongated Mn-sulphide (MnS) inclusions during tensile deformation at elevated temperatures [35]. Jin et al. [36] clarified that variations in the Mn content within 0.04–0.93 (wt%) in low-carbon 9Cr2WVT steel have little effect on the tensile properties of the alloys at various high temperatures.

Fig. 12a shows that the ultimate strength of HSS grades sharply decreases at the onset temperature of 400 °C up to 800 °C. The exception was S690CFD grade steel [13], the degradation of which occurred at a lower rate up to a temperature of 900 °C. The model prediction of the AISC cannot capture the characteristics of the experimental data series of HSS grades, except for SHS700 steel [18] in the temperature range from 550 to 800 °C. The data of CDS 1018 in temperature ranges of 100–300 °C and 650–750 °C lie in the envelope in Fig. 12a, and beyond these temperature ranges, the data lie outside the upper limit of the envelope. The data in Fig. 12b show that the S960QL grade steel [15,16] shows rapid degradation at temperatures higher than 300 °C. The data in both envelopes in Fig. 12b and the curve model predictions of the AISC provide a lower bound for the present data for CDS 1018, except at temperatures above 700 °C. The curve model prediction of the AISC falls on the lower limit of the present data and the narrow upper limit of the envelope.

Wire strand [19] and steel cable [20] with high C contents of 0.81–0.840 wt% were manufactured by the cold-drawing process, and their performances exhibited a dramatic decrease with increasing temperatures, as shown in Fig. 12b. The microstructure of CDS wire steel generally consists of high volume fractions of pearlite and martensite in highly deformed conditions. The interstitial carbon in the body-centred tetragonal (BCT) structure of martensite, which results from carbon decomposition of lamellar pearlite during the cold-drawing process [37], contributes strongly to the extreme strengthening in the wire. Both martensite with a very low plastic deformation capacity [38] and highly deformed lamellar pearlite in the initial microstructure of wire steel have a strongly detrimental effect on fire resistance. Martensite is a well-known metastable phase in steel at high temperature. The carbon atoms in martensite tend to diffuse into the ferrite matrix, where highly deformed pearlite exists. Therefore, interactions between the diffusing carbon atom solutes and deformed lamellar pearlite result in high distortion, which is considered to induce the rapid decrease in wire steel or cable steel properties with increasing temperatures [19,20]. This phenomenon is slightly similar to those of HSS grades [11,14,15] and UHSS grades [15,16] with martensite tempering microstructures. However, somewhat different Q690CFD grade steel [13] and HAS 800 grade steel [14] were manufactured by combinations of TMCP + Q&T treatments, which resulted in slightly better mechanical strength than that of conventional QT HSS grades at elevated temperatures due to the fine martensite grains [11,12,15]. Different behaviour was also observed in hollow steel tubes under cold-forming conditions [18], in which heavy cold-forming results in highly fine grain sizes in the transverse direction [27]. However, the finer grains of the microstructure have opposite effects on the thermal creep resistance.

3.4. Comparative analysis of test results in transient-state condition

Fig. 13a displays comparisons of the reduction in the elastic modulus of AISI 1018 steel under cold-drawing conditions with those of HSS grades under different manufacturing conditions. The data in the envelope reveal that the disparities in the elastic modulus are attributable to the different initial microstructures, which lead to nonlinear elastic behaviour of the steel obtained from transient temperature deformation tests. Therefore, the model predictions of the EC3 and ASCE generally cannot capture the data series of HSS grades in the envelope in Fig. 13a. However, the data of the S690QL grade steel [16] show slightly conservative results relative to the EC3 and the weighted centreline of the envelope in Fig. 13a in temperature range of 450–700 °C. In the temperature range of 100–450 °C, SHS700 [18] shows a slow reduction rate of elastic modulus, and from 500 to 650 °C, it exhibits almost the

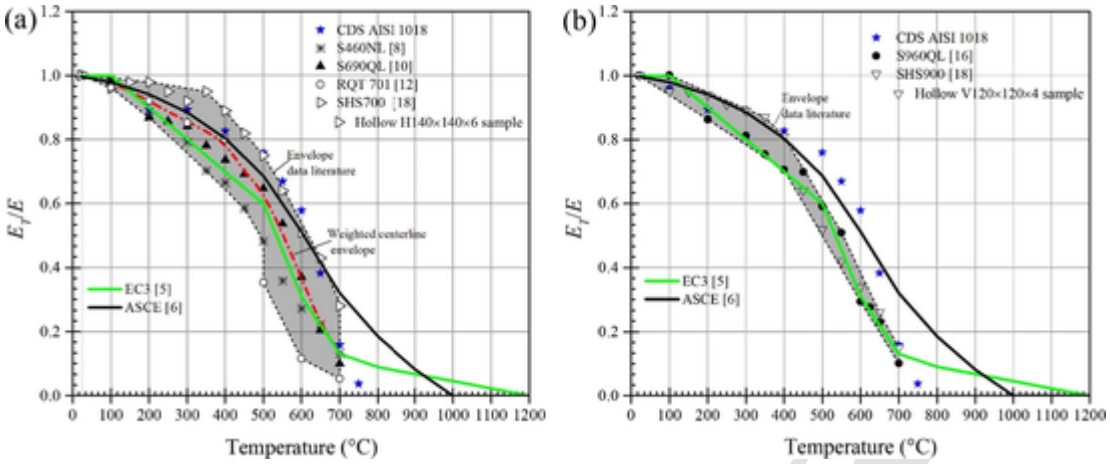

Fig. 13. Comparison of the reduction factor–temperature relationship of the elastic modulus under transient-state conditions for different steel grades (a) $f_y < 700$ and (b) $f_y > 700$.

same rate as CDS 1018. Furthermore, the data for the present test series of CDS 1018 and the data for SHS900 [18] in Fig. 13b are generally conservative relative to the model prediction of the ASCE in the temperature range of 100 to 400 °C. The data for S960QL grade steel [16] show good correlation with the model prediction of the EC3 but not the model prediction of the ASCE, as shown in Fig. 13b.

The data for S460NL grade steel [8] experience markedly slow degradation in temperature range of 100–400 °C, and the reduction in yield strength is lower than the reduction in yield strength of CDS 1018, S690QL steel [10], RQT 701 steel [12] and cold-formed hollow steel tubes (SHS700) [18], as shown in Fig. 14a. The slow degradation of S460NL grade steel followed by rapid degradation in Fig. 14a may be attributed to the formation of finely dispersed particles of carbides containing the micro-alloying elements Nb, Ni or Ti [39,40] in the ferrite matrix. Therefore, the presence of these fine particles has a strengthening effect at ambient temperature and at temperatures up to 400 °C by slowing the recovery in steel. However, a similar effect is not observed in S960QL grade steel [16] containing these strong carbide-forming elements. The data for S960QL grade steel [16] in Fig. 14b reveal that the rapid degradation of yield strength at the onset temperature of 200 °C is due to the presence of martensite structures in the steel. Due to the low thermal stability of martensite at high temperatures, carbon atoms tend to diffuse outward to form weak carbide precipitates containing soluble molybdenum and chromium atoms [15]. The carbides containing solute elements dissolved in the fine particles form large precipitates [41], which can often be considered detrimental to thermal creep resistance, as the precipitates function as a sink for alloying elements that improve the creep resistance [42]. Fig. 14a and b evidently support this explanation, where the data for S690QL steel [10], RQT 701 steel [12] and S960QL grade steel [16] exhibit similar characteristics to the degradation of the mechanical strength in HSS grades at temperatures higher than 300 °C. Rapid degradation is also observable in the hollow steel tube data [18] in Fig. 14a and b, in which the fine grains in the microstructure of the hollow steel tubes under highly cold-formed conditions do not have a positive effect on thermal deformation resistance. Again, the data for CDS 1018 from the present test series exhibit better performance than that exhibited by the data in the envelopes in Fig. 14a and b. Reduction factors of the yield strength predicted using the model predictions of the EC3 [5] and ASCE [6] are generally not suitable for predicting the reduction in yield strength of HSS grades [8,10,12,18] and CDS 1018. The curve model predictions of the EC3 and ASCE generally provide the lower bound values of the envelope data in Fig. 14a. Similarly, the curve model predictions from the EC3 and ASCE in Fig. 14b are nonconservative relative to UHSS grades. Clearly, the strengthening mechanisms in S960QL grade steel treated by a combination of the Q&T process [16], hollow steel tubes produced by the cold-forming process [18] and mild steel produced by the cold-drawing process result in considerable differences in steel properties during fire events.

The ultimate strength data for the present series tests of CDS 1018 lie closely between the lower and upper bounds of the thin envelope in Fig. 15a in the temperature range from 100 to 400 °C. The reduction in the ultimate strength of CDS 1018 is relatively constant up to a tem-

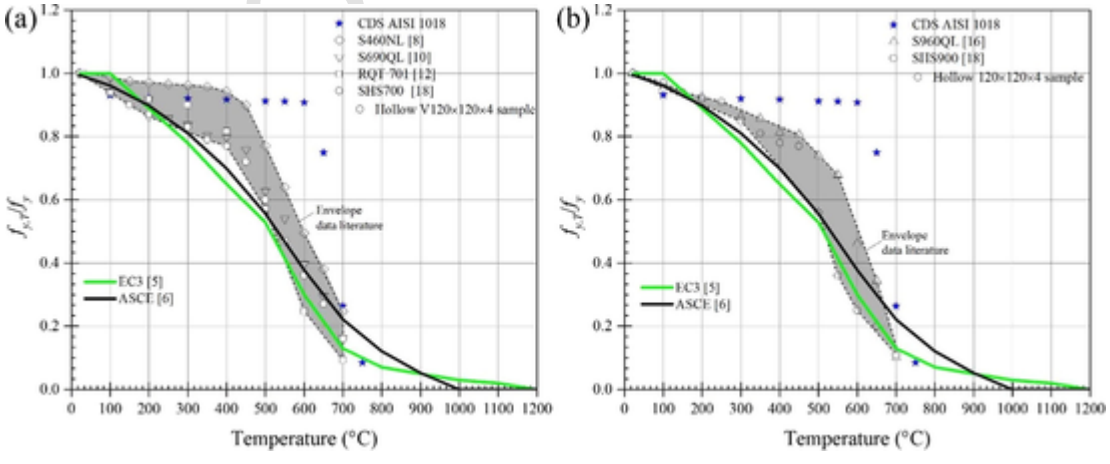

Fig. 14. Comparison of the reduction factor–temperature relationship of the yield strength under transient-state conditions for different steel grades (a) $f_y < 700$ and (b) $f_y > 700$.

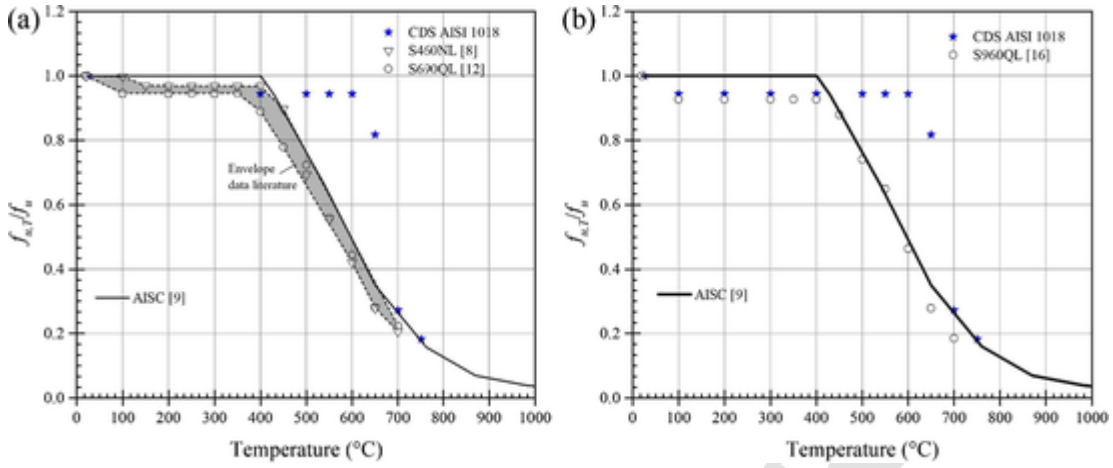

Fig. 15. Comparison of the reduction factor–temperature relationship of the ultimate strength under transient-state conditions for different steel grades (a) $f_y < 700$ and (b) $f_y > 700$.

perature of 600 °C. The elongated grains of ferrite and pearlite along the longitudinal axis of the steel have a positive effect on the thermal creep resistance when the steel is loaded below its yield strength, as shown in Fig. 7. The thermal creep resistance of CDS 1018 up to a temperature of 600 °C may be influenced by the slow rate of dislocation recovery, which results from effective dislocation locking between the coarsening lamellar structures and pinning by the interstitial carbon solute in the ferrite matrix [1]. Temperatures from 500 to 600 °C may cause an increase in the interphase lamellar spacing, which leads to coarsening of the lamellar structures in the pearlite region. In addition, the elongated ferrite and pearlite grains facilitate the many dislocations in the grain interior [43]. The data in the envelope and the present data for CDS 1018 in Fig. 15a are generally below the curve model predictions of the AISC. However, in the temperatures range from 400 to 650 °C, the CDS 1018 data lie above the envelope data and the curve model prediction of the AISC. Similar behaviour is observed for S960 grade steel and CDS 1018 in Fig. 15b. The S960QL grade steel data [16] are conservative relative to the curve model prediction of the AISC in temperature range of 450–600 °C. The comparisons of HSS grades [8,10] and UHSS grade [16] with CDS 1018 in Fig. 15a and b show that the degradation of the mechanical properties of steels at elevated temperatures is dependent on steel manufacturing.

3.5. Failure modes

The typical failure mode of CDS 1018 specimens obtained from high-temperature tension testing in the steady-state condition is displayed in Fig. 16. It can be clearly observed that all specimens experience necking behaviour before failure. CDS 1018 steel exhibited significant necking behaviour at temperatures higher than 600 °C, where the reduction in area increased up to over 50%. For all temperatures tested from 25 °C to 750 °C, CDS 1018 steel does not exhibit brittle failure, which indicates that CDS 1018 shows good performance under steady-state high-temperature conditions.

Furthermore, the typical failure mode of CDS 1018 tensile specimens under transient-state conditions at the stress levels applied in the experimental investigation is shown in Fig. 17. All the steel specimens experienced a necking-down-type tensile failure, indicating typical ductile failure. The steel specimens experienced the highest ductile fracture (a reduction in area ≥~91%) at stress levels of 50–150 MPa, where they failed at temperatures ≥732 °C. Additionally, CDS 1018 steel failed under fire temperatures in excess of 600 °C at fairly low nominal yield stress levels. In both testing methods, for all CDS 1018 steel failure modes, despite a decrease in ductility or an increase in ductility ac-

Fig. 16. Failure modes of CDS AISI 1018 specimens after high-temperature tension testing under steady-state conditions.

companied by a loss of the strain-hardening capacity, the failure remained ductile, as shown in Figs. 16 and 17.

4. Conclusions

The mechanical properties of cold-drawn AISI 1018 steel under steady-state and transient-state conditions at elevated temperatures were experimentally investigated. Data model predictions from the EC2, the EC3 and the ASCE are not appropriate for predicting the thermal expansion of mild steel under cold-drawing conditions, which indicates that the strain-hardening strengthening of mild steel by cold-drawing has a beneficial effect on the relatively slow thermal expansion rate up to a temperature of 650 °C. Generally, under steady-state conditions, the degradation of the mechanical properties of CDS 1018 is relatively higher than that of HSS grades in the temperature range from 100 to 300 °C, but in the temperature range of 400–500 °C, CDS 1018 exhibits a gradual increase in mechanical strength and ductility due to the DSA effect. Under transient-state conditions, CDS 1018 exhibits bet-

Fig. 17. Failure modes of CDS AISI 1018 specimens at different stress levels after transient temperature deformation tests.

ter mechanical strength than that of HSS grades and UHSS grades in the temperature range of 500–600 °C. Generally, significant disparities in the mechanical properties of structural steel in a fire are attributed to the initial microstructure. Mild steel (AISI 1018) under cold-drawing conditions exhibits thermal creep resistance until the fire temperature reaches 600 °C. The elevated temperature data obtained from the present experiment testing programme are applicable to fire-safety design in engineering applications, where the Eurocode, ASCE and AISC model predictions cannot be applied for mild steel under cold-drawing conditions.

Declaration of Competing Interest

The authors declare that they have no known competing financial interests or personal relationships that could have appeared to influence the work reported in this paper.

Acknowledgements

This research was funded by the Directorate of Research and Community Service, the General Directorate of Research Strengthening and Development, the Ministry of Research, Technology, and Higher Education of the Republic of Indonesia under contract No. 065/SP2H/LT/DRPM/2019.

Appendix A. Supplementary data

Supplementary data to this article can be found online at https://doi.org/10.1016/j.conbuildmat.2019.117193.

References

[1] B.R. Kirby, R.R. Preston, High temperature properties of hot-rolled structural steels for use in fire engineering design studies, Fire Saf. J. 13 (1988) 27–37.
[2] J. Chen, B. Young, B. Uy, Behavior of high strength structural steel at elevated temperatures, J. Struct. Eng. 132 (2006) 1948–1954.
[3] M. Knobloch, J. Pauli, M. Fontana, Influence of the strain-rate on the mechanical properties of mild carbon steel at elevated temperatures, Mater. Des. 49 (2013) 553–565.
[4] M. Neuenschwander, M. Knobloch, M. Fontana, Elevated temperature mechanical properties of solid section structural steel, Constr. Build. Mater. 149 (2017) 186–201.
[5] Eurocode 3. ECCS Eurocode Design Manuals: Design of steel Structures, part 1–2, Structural High Temperature Design, European Convention for Constructional Steel Works, first-ed., 2012.
[6] ASCE, Structural Fire Engineering (Structural Division), in: T.T. Lie (Ed.), Structural Fire Protection: Manual of Practice No. 78, American Society of Civil Engineers, New York, NY, United States 1992, pp. 224–225.
[7] T. Ranawaka, M. Mahendran, Experimental study of the mechanical properties of light gauge cold-formed steels at elevated temperatures, Fire Saf. J. 44 (2009) 219–229.
[8] X. Qiang, F. Bijlaard, H. Kolstein, Elevated-temperature mechanical properties of high strength structural steel S460N: experimental study and recommendations for fire-resistance design, Fire Saf. J. 55 (2013) 15–21.
[9] AISC 360, Specification for Structural Steel Building, American Institute of Steel Construction Inc., United States of America, 2005.
[10] X. Qiang, F. Bijlaard, H. Kolstein, Dependence of mechanical properties of high strength steel S690 on elevated temperatures, Constr. Build. Mater. 30 (2012) 73–79.
[11] S.P. Chiew, M.S. Zhao, C.K. Lee, Mechanical properties of heat-treated high strength steel under fire/post-fire conditions, J. Constr. Steel Res. 98 (2014) 12–19.
[12] M.X. Xiong, J.Y.R. Liew, Mechanical properties of heat-treated high tensile structural steel at elevated temperatures, Thin-Walled Struct. 98 (2016) 169–176.
[13] J. Jiang, W. Bao, Z.Y. Peng, Y.B. Wang, J. Liu, X.H. Dai, Experimental investigation on mechanical behaviours of TMCP high strength steel, Constr. Build. Mater. 200 (2019) 664–680.
[14] I.R. Choi, K.S. Chung, D.H. Kim, Thermal and mechanical properties of high strength structural steel HSA800 at elevated temperatures, Mater. Des. 63 (2014) 544–551.
[15] M. Neuenschwander, C. Scandella, M. Knobloch, M. Fontana, Modeling elevated-temperature mechanical behavior of high and ultra-high strength steels in structural fire design, Mater. Des. 136 (2017) 81–102.
[16] X. Qiang, X. Jiang, F.S.K. Bijlaard, H. Kolstein, Mechanical properties and design recommendations of very high strength steel S960 in fire, Eng. Struct. 112 (2016) 60–70.
[17] A. Heidarpour, N.S. Tofts, A.H. Korayem, X.L. Zhao, C.R. Hutchinson, Mechanical properties of very high strength steel at elevated temperatures, Fire Saf. J. 64 (2014) 27–35.
[18] H.T. Li, B. Young, Material properties of cold-formed high strength steel at elevated temperatures, Thin-Walled Struct. 115 (2017) 289–299.
[19] A.M. Shakya, V.K.R. Kodur, Effect of temperature on the mechanical properties of low relaxation seven-wire prestressing strand, Constr. Build. Mater. 124 (2016) 74–84.
[20] Y. Du, J.Z. Peng, J.Y.R. Liew, G.Q. Li, Mechanical properties of high tensile steel cables at elevated temperatures, Constr. Build. Mater. 182 (2018) 52–65.
[21] G. Yuan, Q. Shu, Z. Huang, Q. Li, An experimental investigation of properties of Q345 steel pipe at elevated temperatures, J. Constr. Steel Res. 118 (2016) 41–48.
[22] Eurocode 2: Design of Concrete Structures: Part 1-2: General rules-Structural Fire Design. British Standards Institution, 2004.
[23] ASTM E8, Standard Test Methods for Tension Testing of Metallic Materials, West Conshohocken, United States, 2004.
[24] ASTM E21, Standard Test Methods for Elevated Temperature Tension Tests of Metallic Materials, West Conshohocken, United States, 2005.
[25] ASTM E111, Standard Test Method for Young's Modulus, Tangent Modulus, and Chord Modulus. West Conshohocken, United States, 2004.
[26] Z. Tao, Mechanical properties of prestressing steel after fire exposure, Mater. Struct. 48 (2015) 3037–3047.
[27] J.L. Ma, T.M. Chan, B. Young, Material properties and residual stresses of cold-formed high strength steel hollow sections, J. Constr. Steel Res. 109 (2015) 152–165.
[28] X. Zhang, N. Hansen, A. Godfrey, X. Huang, Dislocation-based plasticity and strengthening mechanisms in sub-20 nm lamellar structures in pearlitic steel wire, Acta Mater. 114 (2016) 176–183.
[29] S. Sato, K. Wagatsuma, S. Suzuki, M. Kumagai, M. Imafuku, H. Tashiro, K. Kajiwara, T. Shobu, Relationship between dislocations and residual stresses in cold-drawn pearlitic steel analyzed by energy-dispersive X-ray diffraction, Mater. Charact. 83 (2013) 152–160.
[30] L. Zhou, F. Fang, L. Wang, H. Chen, Z. Xie, J. Jiang, Torsion delamination and recrystallized cementite of heavy drawing pearlite wires after low temperature annealing, Mater. Sci. Eng. A 713 (2018) 52–60.

[31] L.J. Milovic, T. Vuherer, I. Blacic, M. Vrhovac, M. Stankovic, Microstructures and mechanical properties of creep resistant steel for application at elevated temperatures, Mater. Des. 46 (2013) 660–667.
[32] B.A. Latella, S.R. Humphries, Young's modulus of a 2.25Cr–1Mo steel at elevated temperature, Scr. Mater. 51 (2004) 635–639.
[33] K. Sawada, T. Ohba, H. Kushima, K. Kimura, Effect of microstructure on elastic property at high temperatures in ferritic heat resistant steels, Mater. Sci. Eng. A 394 (2005) 36–42.
[34] B. Park, J.W. Lee, Y.S. Lee, K.T. Park, W.J. Nam, Effects of the annealing temperature and time on the microstructural evolution and corresponding the mechanical properties of cold-drawn steel wires, Met. Mater. Int. 14 (2008) 59–64.
[35] J. Maciejewski, The effects of sulfide inclusions on mechanical properties and failures of steel components, J. Fail. Anal. Preven. 15 (2015) 169–178.
[36] X. Jin, S. Chen, L. Rong, Effects of Mn on the mechanical properties and high temperature oxidation of 9Cr2WVTa steel, J. Nucl. Mater. 494 (2017) 103–113.
[37] S. Djaziri, Y. Li, G. Ali Nematollahi, B. Grabowski, S. Goto, C. Kirchlechner, A. Kostka, S. Doyle, J. Neugebauer, D. Raabe, G. Dehm, Deformation-induced martensite: a new paradigm for exceptional steels, Adv. Mater. 28 (2016) 7753–7757.
[38] M. Badaruddin, Sugiyanto, H. Wardono, Andoko, C.J. Wang, A.K. Rivai, Improvement of low-cycle fatigue resistance in AISI 4140 steel by annealing treatment, Intl. J. Fat. 125 (2019) 406–417.
[39] S. Ghosh, S. Mula, Thermomechanical processing of low carbon Nb–Ti stabilized microalloyed steel: Microstructure and mechanical properties, Mater. Sci. Eng. A 646 (2015) 218–233.
[40] A. Karmakar, S. Biswas, S. Mukherjee, D. Chakrabarti, V. Kumar, Effect of composition and thermo-mechanical processing schedule on the microstructure, precipitation and strengthening of Nb-microalloyed steel, Mater. Sci. Eng. A 690 (2017) 158–169.
[41] H. Hirata, K. Ogawa, Effect of carbon content on creep rupture strength and microstructure in heat affected zone of heat resistant ferritic steel: alleviation of decrease in creep rupture strength in heat affected zone of heat resistant ferritic steel, Sci. Technol. Weld. Join. 13 (2008) 524–532.
[42] S. Karthikeyan, G.B. Viswanathan, P.I. Gouma, V.K. Vasudevan, Y.W. Kim, M.J. Mills, Mechanisms and effect of microstructure on creep of TiAl-based alloys, Mater. Sci. Eng. A 329–331 (2002) 621–630.
[43] B.N. Jaya, S. Goto, G. Richter, C. Kirchlechner, G. Dehm, Fracture behavior of nanostructured heavily cold drawn pearlitic steel wires before and after annealing, Mater. Sci. Eng. A 707 (2017) 164–171.